

Unveiling spatial and temporal heterogeneity of a tropical forest canopy using high-resolution NIRv, FCVI, and NIRvrad from UAS observations

Trina Merrick^{1,4,8*}, Stephanie Pau¹, Matteo Detto^{2,3}, Eben N. Broadbent⁴, Stephanie A. Bohlman^{2,5}, Christopher J. Still⁶, Angelica M. Almeyda Zambrano⁷

¹ Department of Geography, Florida State University, 113 Collegiate Loop, Tallahassee, Florida 32306, USA

² Smithsonian Tropical Research Institute, Apartado 0843–03092, Balboa, Ancon, Panama

³ Department of Ecology and Evolutionary Biology, Princeton University, Princeton, New Jersey 08544 USA

⁴ Spatial Ecology and Conservation Lab, School of Forest, Fisheries and Geomatics Sciences, University of Florida, Gainesville, FL, 32608 USA

⁵ School of Forest, Fisheries and Geomatics Sciences, University of Florida, Gainesville, FL, 32608 USA

⁶ Department of Forest Ecosystems and Society, Oregon State University, Corvallis, Oregon 97331 USA

⁷ Spatial Ecology and Conservation Lab, Center for Latin American Studies, University of Florida, Gainesville, Florida 32608 USA

⁸ Naval Research Laboratory, Remote Sensing Division, 4555 Overlook Ave. SW, Washington, DC, 20375, USA

**Author's current location*

Correspondence to: Trina Merrick (trina.merrick@nrl.navy.mil)

Abstract. Recently, remotely-sensed measurements of the near-infrared reflectance (NIRv) of vegetation, the fluorescence correction vegetation index (FCVI), and radiance (NIRvrad) of vegetation, have emerged as indicators of vegetation structure and function with potential to enhance or improve upon commonly used indicators, such as the normalized difference vegetation index (NDVI) and the enhanced vegetation index (EVI). The applicability of these remotely sensed indices to tropical forests, key ecosystems for global carbon and biodiversity, have been limited. In particular, fine-scale spatial and temporal heterogeneity of structure and physiology may contribute to variation in these indices and the properties, such as gross primary productivity (GPP) and absorbed photosynthetically active radiation (APAR), that are presumed to be measured by these indices. In this study, fine-scale (15cm and greater) tropical forest heterogeneity represented by NIRv, FCVI, and NIRvrad, is investigated using unoccupied aerial systems (UAS) data, and compared to NDVI, EVI, and Lidar. By exploiting near-infrared signals, emerging vegetation indicators captured the greatest spatiotemporal variability, followed by the enhanced vegetation index (EVI), then the normalized difference vegetation index (NDVI). Wavelet analyses showed the dominant spatial scale of variability of all indicators is driven by tree clusters and larger-than-tree-crown size gaps rather than individual tree crowns. Emerging indices and EVI captured variability at smaller spatial scales (~50 m) than NDVI (~90 m) and lidar (~70 m). We show that spatial and temporal patterns of NIRv and FCVI are virtually identical for a dense green canopy, confirming predictions in earlier studies. Furthermore, we show that NIRvrad, which does not require separate irradiance measurements, correlated more strongly with GPP and PAR than did other indicators. These emerging indicators, which are related to canopy structure and the radiation regime of vegetation canopies, are promising tools to improve understanding of tropical forest canopy structure and function.

37 1 Introduction

38 Important spatial and temporal heterogeneity in structurally complex and species-rich tropical forests are not
39 well characterized. Many factors, including varying microclimate, light conditions, topography, crown structure, and
40 patterns of tree mortality and regeneration, contribute to high heterogeneity that underlies coarse scale gross primary
41 production (GPP) measurements in tropical forest (e.g., Xu et al., 2015; Guan et al., 2015; Morton et al., 2014;
42 Bohlman and Pacala, 2012; Laurance et al., 2012; Clark et al., 2008; Huete et al., 2008). Improving knowledge of
43 tropical forest dynamics at multiple scales is crucial to monitoring and predicting resilience of tropical ecosystems
44 and productivity under climate change (Liu et al., 2021; Clark et al., 2017; Laurance et al., 2012; Malhi, 2012; Wright,
45 2010; Saatchi et al., 2010; Lewis et al., 2009). Remote sensing (RS) measurements have been employed to uncover
46 vegetation patterns of structure and productivity from local to global scales, often with a focus on filling gaps in
47 knowledge regarding variation and uncertainties in GPP estimates (e.g., Jung et al., 2011; Glenn et al., 2008; Huete et
48 al., 2002; Ryu et al., 2018; Yang et al., 2017; Jiang et al., 2008; Zhao et al., 2010; Heinsch et al., 2006; Running et al.,
49 2004; Turner et al., 2003). Yet, there is a spatial mismatch between satellite data (e.g., 30 m to 1 km pixel resolution),
50 which provides observations across large extents at repeat intervals, and site-specific plot level data (e.g., 0.1 – 1
51 hectare) that contributes to uncertainties in GPP estimates (Gelybó et al., 2013; Zhang et al., 2020). There is a lack of
52 high spatial and temporal resolution data that can capture fine-grained heterogeneity of tropical forests (Clark et al.,
53 2017; Mitchard, 2018; Saatchi et al., 2011; Lewis et al., 2009). Unoccupied aerial systems (UAS) with hyperspectral
54 imaging sensors present an opportunity to collect tropical forest canopy data at high spatial resolution, which could
55 address unknowns related to the high heterogeneity of tropical forests.

56 Traditional reflectance-based indices (RI) using RS data, such as the normalized difference vegetation index
57 (NDVI) and enhanced vegetation index (EVI), are known to capture structural changes that are coincident with
58 changes in GPP. RIs have provided optical methods using RS to track GPP via the light use efficiency (LUE) model
59 (J.L.Monteith, 1977; Yuan et al., 2014; B. E. Medlyn, 1998). In the most commonly used formulation of the LUE
60 model for RS, GPP is the product of the absorbed photosynthetically active radiation (APAR) and the efficiency (ϵ)
61 with which the target vegetation converts the radiation to carbon (Gamon, 2015; Yuan et al., 2014; Running et al.,
62 2004). APAR is derived from the incoming photosynthetically active radiation (PAR) times the fraction of PAR
63 (fPAR). RIs commonly used in the LUE model of GPP as well as direct proxies for GPP are NDVI and EVI, because
64 of a strong relationship to fPAR (Springer et al., 2017; Morton et al., 2015; Gamon et al., 2015; Porcar-Castell et al.,
65 2014; Glenn et al., 2008; Gao et al., 2007; Huete et al., 2002; Zarco-Tejada et al., 2013). NDVI and EVI are typically
66 used as proxies on seasonal timescales, or, when used to examine changes on shorter timescales, they have been
67 multiplied by photosynthetically active radiation (PAR) to account for changes in radiation (incoming, absorbed, and
68 scattered) which better align with GPP changes (Springer et al., 2017; Yuan et al., 2014). However, RIs alone have
69 often not shown enough sensitivity to capture more fine-scale or rapid changes in vegetation, such as those in tropical
70 forests, and questions linger about the ability to track green-up with RIs in tropical regions (Liu et al., 2021; Yang et
71 al., 2018a; Lee et al., 2013; Xu et al., 2015; Morton et al., 2014; Samanta et al., 2010; Sims et al., 2008).

72 Recently, three emerging vegetation indicators have been shown to track with GPP more closely than traditional
73 RIs. These indicators are the near-infrared reflectance of vegetation (NIRv) (Badgley et al., 2017), the fluorescence

74 correction vegetation index (FCVI) (Yang et al., 2020) and the near-infrared radiance of vegetation (NIRvrad) (Wu et
75 al., 2020). Because they exploit additional information from the NIR region of the spectrum, NIRv, FCVI, and
76 NIRvrad do not saturate in dense canopies or suffer the same level of contamination from senesced vegetation and
77 soils as traditional RIs (Baldocchi et al., 2020; Badgley et al., 2017). Additionally, these emerging indicators require
78 only moderate spectral resolution data and are similarly straightforward to measure and calculate as RIs, making them
79 accessible in a broad range of studies. In contrast, SIF measurements require very high spectral resolution and multiple
80 instruments. Therefore, NIRv, FCVI, and NIRvrad could be employed as valuable indicators of canopy structure and
81 function (Badgley et al., 2019; Badgley et al., 2017; Dechant et al., 2020) and have practical advantages over making
82 SIF measurements.

83 NIRv, the product of NDVI and the near-infrared reflectance (NIR), from moderate spectral resolution
84 satellite imagery and field spectrometers has been shown to empirically track measured and modelled GPP globally
85 (with highest uncertainties in the tropics) at monthly to seasonal timescales presumably because changes in canopy
86 phenology influence light capture and these changes coincide with changes in GPP (Badgley et al., 2019; Badgley et
87 al., 2017; Dechant et al., 2020). FCVI, derived from radiative transfer theory rather than an empirical relationship, is
88 calculated from RS data by subtracting the reflectance in the NIR from the reflectance in the visible range (Yang et
89 al., 2020). Yang et al. (2020) demonstrated that FCVI, by capturing structure and radiation information from a
90 vegetated canopy, tracked GPP and solar-induced fluorescence (SIF; a radiance-based indicator of GPP) in field
91 experiments with crops and in numerical experiments. Yet FCVI showed differences from NIRv due to exposed soil
92 within the vegetated study areas. In previous studies, FCVI and NIRv were similar for dense green canopies where
93 soils have less of an impact, but this has not yet been tested in the tropics (Wang et al., 2020; Badgley et al., 2019;
94 Dechant et al., 2020). NIRvrad was proposed as a proxy for GPP on half-hourly and daily timescales, in contrast to
95 NIRv and FCVI which track changes on longer timescales (Wu et al., 2020; Dechant et al., 2020; Baldocchi et al.,
96 2020; Zeng et al., 2019). NIRvrad is calculated by multiplying NDVI by the NIR radiance, and because the radiance
97 of NIR accounts for incoming radiation at short timescales, has tracked GPP and SIF on half-hourly and diurnal scales
98 as well as seasonally in crops and, to a limited extent, natural grass and savanna ecosystems (Dechant et al., 2020;
99 Baldocchi et al., 2020; Zeng et al., 2019; Wu et al., 2020).

100 Readily available UAS-based hyperspectral sensors are capable of robust measurements of NIRv, FCVI, and
101 NIRvrad at ultra-high spatial scales, i.e. in tens of centimeters. In this regard, UAS-based data have the potential to
102 improve our understanding of tropical forest structure and function over a range of scales that are poorly resolved by
103 other RS platforms. Here, we use high spatial resolution UAS measurements to characterize spatial and temporal
104 variation in a semi-deciduous tropical forest canopy during the dry season, and compare commonly used spectral
105 indices (NDVI and EVI) to newer vegetation indicators (NIRv, NIRvrad, and FCVI) by (i) examining correlations
106 between GPP and vegetation indicators using mean values across the canopy throughout the day, (ii) evaluating the
107 distribution of fine spatial resolution values (~15 cm) across the canopy and examining changes in this spatial variation
108 throughout the course of two days, and finally (iii) identifying the dominant spatial scale driving variation across our
109 10 ha study region.

110 2 Materials and Methods

111 2.1 Study Area

112 Barro Colorado Island (BCI), Panama, is a 1560 ha island (approximately 15 km²) in Gatun Lake, which was formed
113 by the construction of the Panama Canal. The Smithsonian Tropical Research Institute manages the preserved area
114 specifically for research. This semi-deciduous moist tropical forest receives approximately 2640 mm mean annual
115 precipitation and has a mean temperature of 26°C with a dry season from approximately January through April (Detto
116 et al., 2018). There is high species diversity, with approximately 500 tree species, approximately 60 species per ha,
117 and about 6.3% of trees at >30cm diameter at breast height (dbh) (Bohlman and O'Brien, 2006; Condit et al., 2000).
118 The UAS and ground measurements were focused on an area approximately 10 ha within the footprint of an eddy
119 covariance tower near the center of the island (9.156440°, -79.848210°).

120 2.2 Data collection

121 The GatorEye Unmanned Flying Laboratory is a hardware and software system built for sensor fusion
122 applications, and which includes hyperspectral, thermal, and visual cameras and a Lidar sensor, coupled with a
123 differential GNSS, internal hard drives, computing systems, and an Inertial Motion Unit (IMU). Hardware and
124 processing details, as well as data downloads, are available at www.gatoreye.org. The GatorEye flew 13 missions on
125 January 30 and 31, 2019 over the forest canopy within the eddy covariance tower footprint at an average height of 120
126 m above ground level (AGL) and at 12 m/s (Fig. 1). In this study, we used radiometrically calibrated flight transects
127 from the Nano VNIR 270 spectral band hyperspectral sensor (Headwall Photonics, Fitchburg, MA, USA) which
128 covered approximately 1 ha per flight within the EC footprint in this study. The Nano spectrally samples at
129 approximately 2.2 nm and 12-bit radiometric resolution from 400 to 1050 nm. The frame rate was set to 100 fps, with
130 an integration time of 12 ms and provided a pixel resolution of approximately 15x15 cm. The Nano was calibrated to
131 radiance by the manufacturer before the field campaign and pixel drift was removed by dark images collection, which
132 was corrected for during the conversion from digital number to radiance. The hyperspectral transects were equally
133 subset for each flight in ENVI + IDL (Harris Geospatial, Boulder, CO). Each flight resulted in 1920 transects of
134 approximately 400 m length composing three blocks discretized in 2500 data points. Simultaneous lidar was collected
135 using a VLP-32c ultra puck (Velodyne, San Jose, CA), which was processed to a 0.5x0.5 m resolution digital surface
136 model (DSM).

137 Turbulent fluxes and meteorological variables were measured from a 40 m Eddy Covariance (EC) flux tower
138 (Fig. 1). The eddy covariance system includes a sonic anemometer (CSAT3, Campbell Scientific, Logan, UT) and an
139 open-path infrared CO₂/H₂O gas analyzer (LI7500, LiCOR, Lincoln, NE). High-frequency (10Hz) measurements
140 were acquired by a datalogger (CR1000, Campbell Scientific) and stored on a local PC. Other measurements made at
141 the tower include air temperature and relative humidity (HC2S3, Rotronic, Hauppauge New York), and
142 photosynthetically active radiation (PAR; BF5, Delta-T Devices, UK). EC data were processed with a custom program
143 using a standard routine described in Detto et al. (2010). GPP was derived from daytime values of NEE by adding the
144 corresponding mean daily ecosystem respiration obtained as the intercept of the light response curve (Lasslop et al.,

145 2010). Due to a power issue, data corresponding to the January 30 flights was not collected, so only January 30 GPP
146 were available.

147 An HH2 Pro Spectroradiometer (HH2; ASD/Panalytical/Malvern, Boulder, CO) fitted with a diffuse cosine
148 receptor was used on the ground in full sun at the forest edge to record incoming irradiance on January 30 and 31,
149 2019 (~ 3nm FWHM and spectral sampling at 1nm). HH2 irradiance was resampled to match the Nano hyperspectral
150 sensor and used to calculate reflectance. A calibrated reference tarp was placed in full sun at the forest edge and the
151 UAS flew over and recorded the tarp each UAS flight. Reflectance was calculated separately using the HH2 and tarp
152 data and resulting reflectance values compared as a method to vicariously cross-calibrate reflectance from the
153 hyperspectral data (<7.0% difference for all data in the study). In addition, PAR was calculated with the HH2 data and
154 compared to the tower-mounted PAR measurement (approximately 1.5 km apart) to help understand any differences
155 in the sky conditions during flight times. PAR differences across the site for each flight time for the duration of flights
156 (approximately 10-15 minutes in length each) ranged between 4.0% and 10.3%. A summary of materials and methods
157 is provided in Fig.1 at the end of Section 2.

158

159 2.3 Vegetation indicators

160 We calculated NDVI and EVI as (Tucker, 1979; Huete et al., 2002; Rouse JR et al., 1974):

$$161 \quad NDVI = \frac{R_{770-800} - R_{630-670}}{R_{770-800} + R_{630-670}} \quad (1)$$

161 and

$$162 \quad EVI = \frac{2.5(R_{770-800} - R_{630-670})}{R_{770-800} + 6 \times R_{630-670} - 6 \times R_{460-475} + 1} \quad (2)$$

162 where R is reflectance and the subscripts indicate wavelengths. Here, we used the averages of 770-800 nm for NIR,
163 630-670 nm for red reflectance, and 460-475 nm for blue bands reflectance and normalized to reduce noise.

164 We further calculated the near-infrared vegetation index NIRv as:

$$165 \quad NIRv = NDVI \times R_{770-800} \quad (3)$$

165 where R₇₇₀₋₈₀₀ is the NIR reflectance (Badgley et al., 2017). The fluorescence correction vegetation index (FCVI)
166 was calculated from spectral data by subtracting the reflectance in the visible range (R₄₀₀₋₇₀₀) from the NIR
167 reflectance (Yang et al., 2020) as follows

$$168 \quad FCVI = R_{770-800} - R_{400-700} \quad (4).$$

168 The near-infrared radiance of vegetation (NIRvrad) was calculated similarly to the NIRv, except NDVI was multiplied
169 by the radiance, rather than reflectance, from the NIR region (Rad₇₇₀₋₈₀₀) (Wu et al., 2020) as follows:

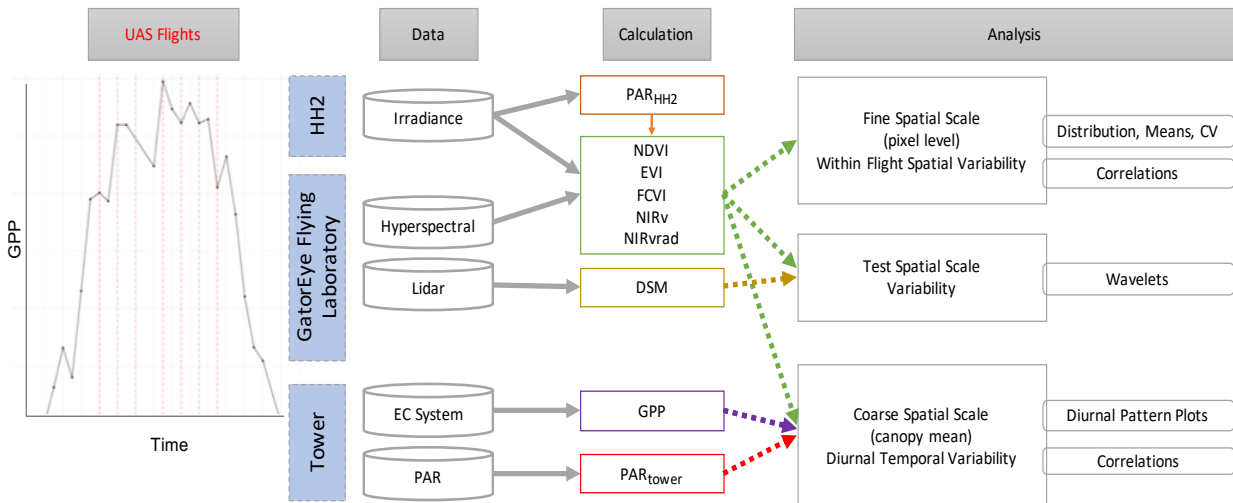
$$170 \quad NIRvrad = NDVI \times Rad_{770-800} \quad (5).$$

170 2.4 Data Analysis

171 We examined mean values across the canopy over the course of one day by creating a diurnal time series of
172 scatterplots of the tower-based PAR data, tower-based GPP data, and means of all spectral vegetation indicators, on

173 Jan 31, 2019, and ran comparisons using Pearson’s correlation coefficients to examine correlations. At fine spatial
 174 scales, i.e. pixel level of ~15 cm, we created density plots, calculated the coefficient of variation (CV), and calculated
 175 the means of all vegetation indicators (NDVI, EVI, NIRv, FCVI, NIRvrad) for each flight to compare spatial and
 176 temporal variability (Fig. 1). To determine which spatial scales dominate the variability of each vegetation quantity,
 177 we ran power spectrum wavelet analysis using code created in the Matlab programming language (Mathworks, Natick,
 178 Massachusetts). For each vegetation quantity and each flight, and for the lidar elevation model representing canopy
 179 height, we computed the Morlet wavelet power spectrum of individual transects (Torrence and Compo, 1998). All
 180 power spectra from the wavelet analysis were normalized to unit variance. An ensemble power spectrum for each
 181 vegetation indicator was created by averaging across all the transects of each flight and then across flights. We then
 182 compared the power spectra for each vegetation indicator and lidar data to compare the spatial scales at which the
 183 quantities captured variability as well as the spatial scale at which the lidar-based elevation model captured variability.
 184 For illustration purposes, Fig. S3 is an example of two signals, a higher and lower noise signal created with fractals
 185 (Signal A and B, respectively, Fig. A1) and the corresponding power spectra which decay differently at smaller spatial
 186 scales (Power Spectra, Fig. A1). Initial UAS data processing was carried out in Interactive Data Language (IDL) and
 187 Environment for Visualizing Images (ENVI) (Harris Geospatial, Boulder, CO). Other analysis, including graphical
 188 illustrations, were carried out using the R open source environment with libraries dplyr, ggplot, and tidyverse (R
 189 Development Core Team, 2010; Wickham et al., 2018; Wickham, 2017, 2016) and Matlab (Mathworks, Natick,
 190 Massachusetts).

191



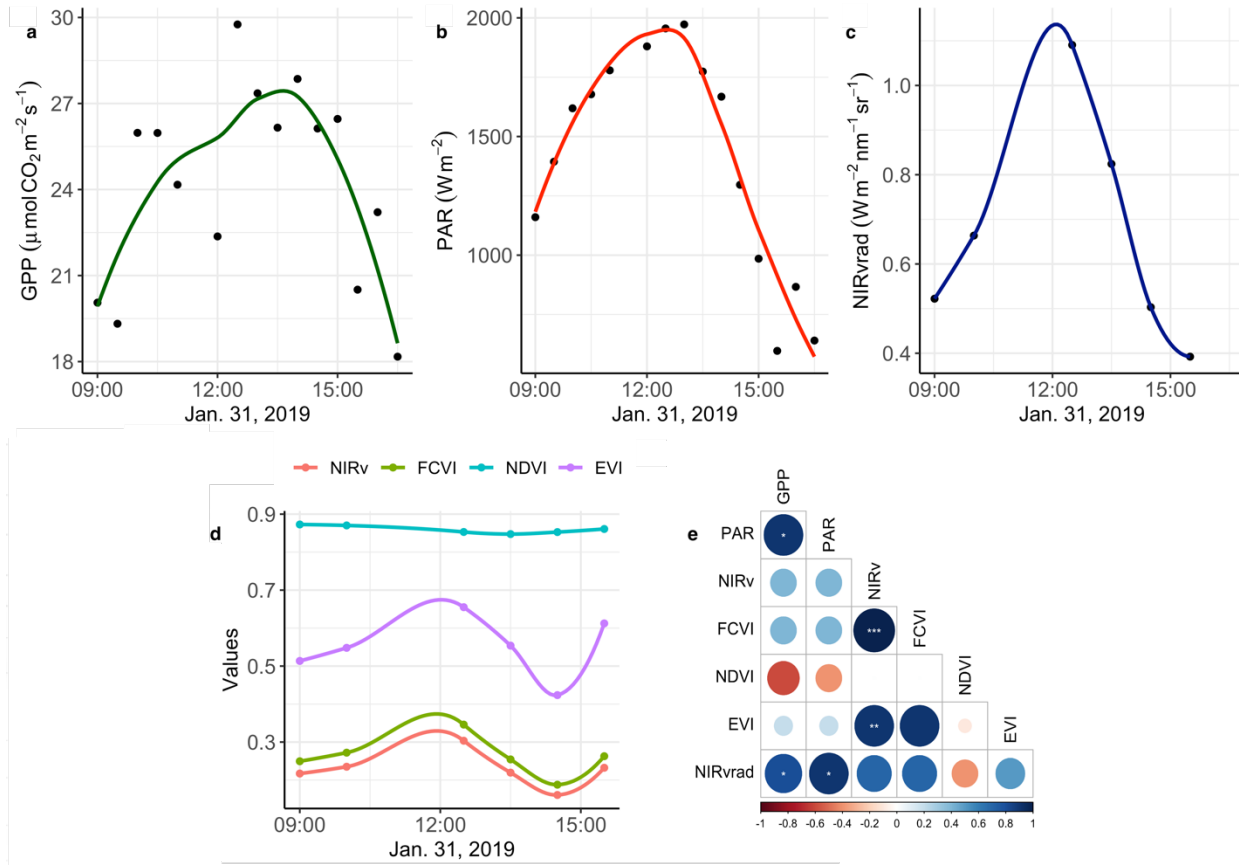
192

193 **Figure 1.** Summary of methods. Concept of diurnal GPP and UAS flights (far left). Platforms and instrumentation (blue)
 194 consisted of the Analytical Spectral Devices (ASD) Handheld Spectroradiometer Pro 2 (HH2), the GatorEye Flying
 195 Laboratory, and the Tower at Barro Colorado Island (BCI). Data collected included Irradiance, Hyperspectral, Lidar,
 196 Eddy Covariance System (EC), and Photosynthetically Active Radiation (PAR). Calculations made were PAR with the HH2
 197 (PAR_{HH2}), the Normalized Difference Vegetation Index (NDVI), Enhanced Vegetation Index (EVI), Fluorescence
 198 Correction Vegetation Index (FCVI), the Near Infrared Vegetation Index (NIRv), the Near Infrared Radiance of Vegetation
 199 (NIRvrad), the Digital Surface Model (DSM), Gross Primary Productivity (GPP) and PAR from the PAR Sensor on the
 200 Tower (PAR_{tower}). An overview of the data analysis at each scale is provided in the right of the diagram.

201 **3 Results and discussion**

202 **3.1 Diurnal trend in spectral vegetation indicators, PAR, and GPP**

203 The degree to which remote sensing vegetation indicators represent changes in GPP depend largely on canopy
204 structure-dependent light absorption and scattering processes, that is, a joint relationship between a remote sensing
205 vegetation quantity, PAR or APAR, and GPP. Fig. 2 shows GPP, PAR, and the mean value of each vegetation quantity
206 at each flight time over the course of January 31, the day on which we had overlapping data between the UAS and
207 eddy covariance system (Fig. 2a-d). Additionally, Pearson correlation coefficients among mean NIRv, FCVI,
208 NIRvrad, EVI, and NDVI for each flight time and the GPP and PAR values at the flight times are shown in Fig. 2d.
209 NIRv is significantly and strongly positively correlated to both FCVI ($r=0.9$, $p<0.001$) and EVI ($r=0.9$, $p<0.01$).
210 NIRvrad is the only vegetation quantity with a significant correlation to PAR and GPP, with a strong positive
211 relationship (0.9 and 0.81, respectively, p-values <0.05 ; Fig. 2d). Mean NIRvrad values also have the greatest relative
212 diurnal change among the vegetation indicators (Fig. 2c and d). These results demonstrate that a shared correlation of
213 NIRvrad and GPP to PAR results in mean NIRvrad tracking diurnal changes in GPP to a greater degree than NIRv,
214 FCVI, NDVI or EVI, because NIRvrad takes incoming radiation into account whereas the other vegetation indicators
215 do not. This evidence – albeit based on only one day of data – supports the proposed use of NIRvrad as a proxy for
216 changes in GPP on short timescales. NIRvrad is also a more efficient measurement of GPP in the sense that a separate
217 instrument to measure PAR is not needed (Wu et al., 2020; Zeng et al., 2019). Given that the relationship between
218 NIRvrad and GPP depends on PAR, it is unclear if the association between NIRvrad and GPP would weaken during
219 the wet season when low light or diffuse light conditions are more common (Berry and Goldsmith, 2020).



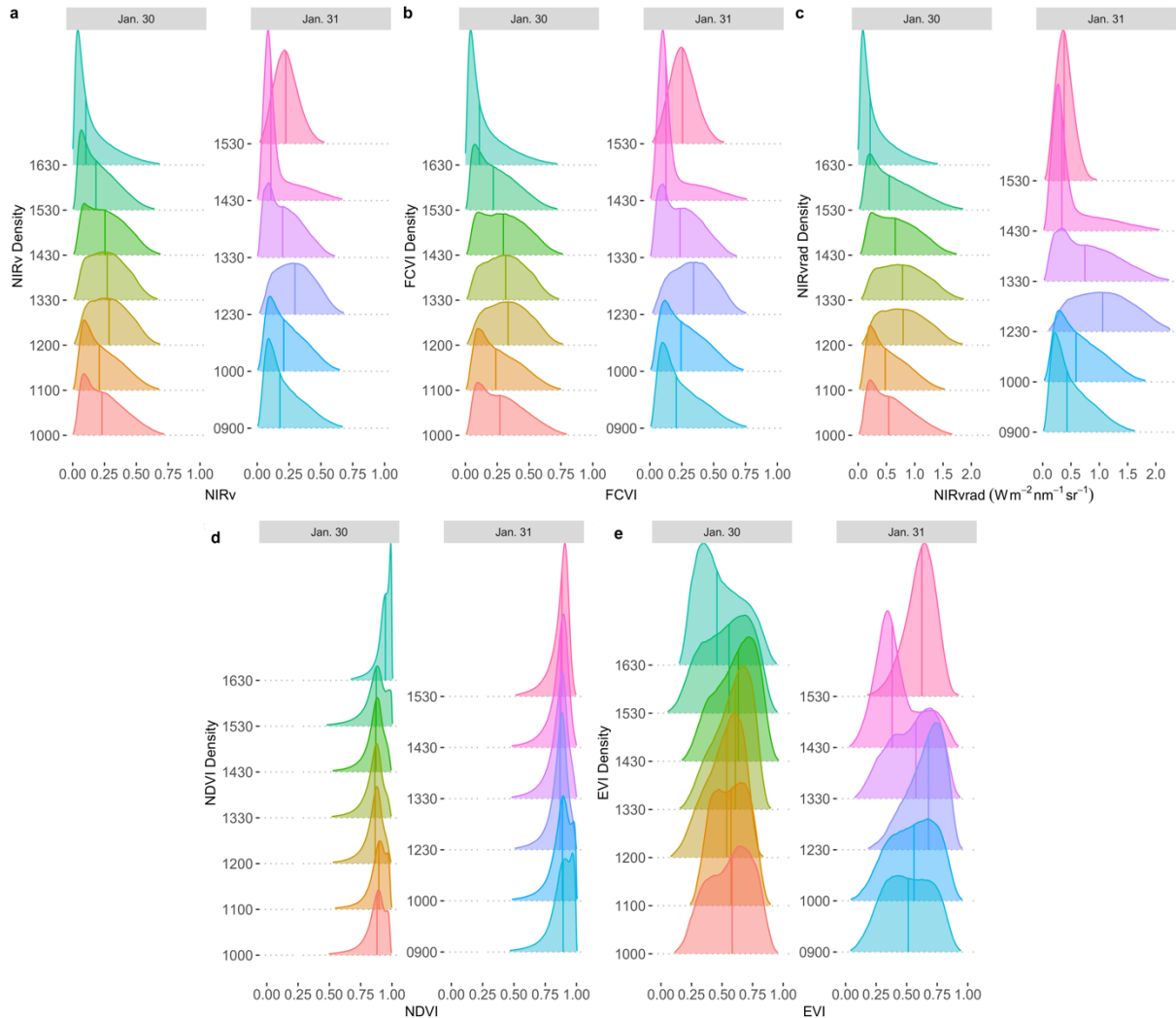
220
 221 **Fig. 2. Diurnal time series of a) GPP b) PAR c) NIRvrad d) NIRv, FCVI, NDVI, and EVI e) comparisons of quantities using**
 222 **Pearson correlations color indicates strength of relationship, * = p-value<0.05, ** = p-value <0.01, *** = p-value <0.001.**

223 **3.2 Tropical forest canopy variation**

224 Spatial distributions and CV of all pixels of NIRv, FCVI, and NIRvrad are generally similar to one another
 225 and show considerable variation spatially across the canopy and temporally over the course of a day and across days
 226 (Fig. 3a-c, Table A2). NIRv, FCVI, and NIRvrad distributions are distinct from EVI and NDVI (Fig. 3a-e, Table A2,
 227 and Table A2). NIRv, FCVI, and NIRvrad have the highest CV at each flight time (between 39.78% and 91.54%,
 228 Table A1), followed by EVI (between 20.24% and 37.24%, Table A2) and NDVI varied the least at any flight time
 229 (between 9.83% and 12.82%, Table A2). For some indices, mean values across the canopy fail to capture extreme
 230 high (NIRv, NIRvrad, and FCVI) or low values (NDVI) during morning and afternoon hours. This pattern suggests
 231 “hot” and “cool” spots of activity related to heterogeneity in forest structure and low sun angles. In previous studies,
 232 the directional effects on NIRv have been examined on coarse spatial scales (i.e. satellites) and have been proposed
 233 as a means of improving understanding of NIRv agreement to GPP (Hao et al., 2021; Dechant et al., 2020; Baldocchi
 234 et al., 2020; Zhang et al., 2020). Our results demonstrate that NIRv, FCVI, and NIRvrad capture fine-grained
 235 heterogeneity of this tropical forest canopy, which was obscured by EVI and NDVI (Fig. 3a-e). NIRv and NIRvrad
 236 use NDVI, thus, by definition, NIR is the largest contributing factor to the heterogeneity captured (Fig. 3a, c, and e).
 237 While NIRv and NIRvrad distributions are generally similar, they diverge in the afternoons when PAR declines, which
 238 likely why NIRvrad is better correlated with GPP. EVI variability was higher than NDVI variability, but lower than

239 that of NIR_v, FCVI, and NIR_{vrad}, indicating that EVI has a different level of sensitivity to viewing geometry and
240 canopy components (potentially understory), light absorption and scattering regime of the canopy than the other
241 indices (Table A1 and Table A2). We also show empirically that NIR_v and FCVI are virtually the same in a dense
242 tropical forest presumably due to both indices similarly representing the radiation regime of the tropical forest canopy,
243 i.e. light capture and scattering, in conditions with little background soil, supporting the predictions of earlier studies
244 (Dechant et al., 2020; Zeng et al., 2019; Yang et al., 2018b; Wu et al., 2020).

245 Midday distributions of NIR_v, FCVI, and NIR_{vrad} on Jan. 30 at 12:00 and 1330 and Jan. 31 at 12:30 are less
246 skewed than at other times of the day whereas morning and afternoon distributions are skewed toward lower values,
247 except for Jan. 31 at 15:30 (Fig. 3a-c). On both days, when mean values peak at midday, the variation for all vegetation
248 indicators is lowest (Jan 30, 1200 CV between 47.6 and 49.2 and Jan 31, 1230 CV between 45.6 and 47.2) (Fig. 3,
249 Table A1). The highest variability occurred in the afternoon on both days (Jan 30, 1630 CV between 91.3% and 91.5
250 and Jan 31, 1430 CV between 83.3% and 83.8% for all quantities) (Fig. 3, Table A2). At midday, NIR_v, FCVI, and
251 NIR_{vrad} variability was low and means were high, indicating that viewing and sun geometry drive the higher and
252 lower values during morning and afternoon. This effect is greater in the afternoon than the morning (Fig. 3, Table
253 A2). However, a different pattern is apparent on Jan. 31 during the 1530 flight time when mean values increased from
254 the 1430 flight time means and the CV values were the lowest of any flight observations in the study and this influence
255 appears to be greatest on EVI. It is possible that this was due to another type of effect on illumination geometry, such
256 as wind influencing the UAS, diffuse radiation effects, or hotspot effects.



257
 258 **Fig. 3.** NIRv (a), FCVI (b), and NIRvrad (c) density plots for each flight time on January 30, 2019 (column 1 each panel)
 259 and January 31 (column 2 each panel). Colours of distributions indicate the flight time and day.

260 **3.3 Power Spectrum Analysis**

261 Power spectrum analysis was used to identify the dominant spatial scales driving variability across the canopy
 262 (Fig. 4). In Fig. 4, the area beneath the curve is proportional to the variance because it is the spectrum divided by the
 263 corresponding scale and then plotted as a function of the log of the scale (example signals and power spectra provided
 264 Fig. A1). Similar to their spatial distributions (Fig. 3), NIRvrad and FCVI are indistinguishable in their dominant
 265 scales of spatial variability (Fig. 3) (Dechant et al., 2020; Zeng et al., 2019). Power spectrum analysis shows a distinct
 266 peak around 50 m spatial scale for NIRv, NIRvrad, FCVI, and EVI, whereas NDVI peaks at approximately 90 m. The
 267 largest tree crown sizes on BCI are on the order of 20-30 m in diameter and the most common crown sizes are between
 268 4-10 m (Fig. A2). Thus, the spatial variability of the vegetation indicators is strongly influenced by larger forest
 269 structures, such as forest gaps and tree clusters, rather than individual tree crowns.

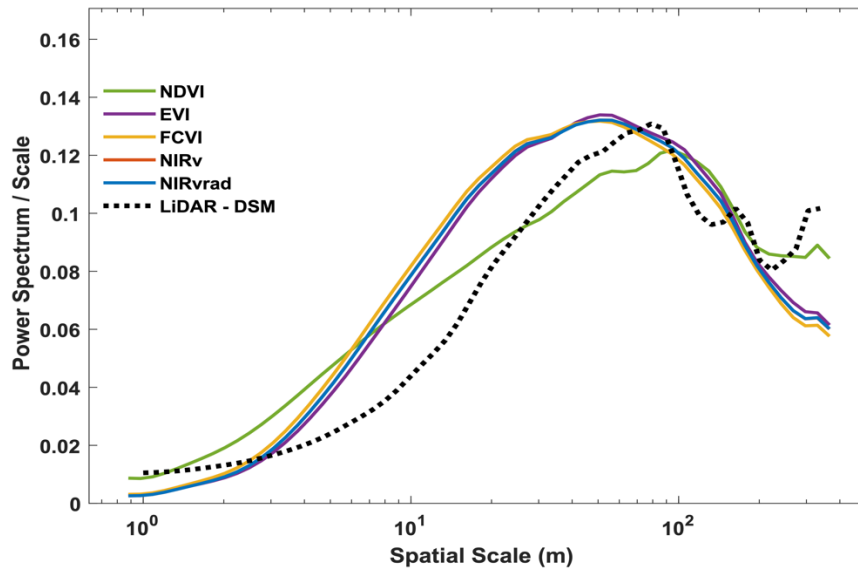
270 This larger scale of variability is also confirmed by the power spectrum of the lidar-derived canopy surface
 271 model, which displays a peak at 70 m scale, indicating that larger than tree crown scales produce the most variability

272 in canopy height. In other words, UAS-based lidar data also show that canopy heights within a 70 m spatial scale
273 create strong spatial features on the landscape. Vegetation indicators and the lidar canopy surface model appear less
274 effective at capturing smaller scale differences within a canopy (leaves or leaf clumps) or among the most frequent
275 tree crown sizes on BCI (4-10 m sunlit tree crown sizes determined by stereophotos; Fig. A2). However, the peaks in
276 the vegetation indicators are broader than the peak in the lidar data, showing that smaller features of the canopy are
277 still contributing to the total spatial signal in the power spectra. These results suggest that satellite data with a spatial
278 resolution greater than ~50 m may miss important variation in diverse tropical forest canopies. NDVI displays a
279 different shape with a slower decay at small scales, indicating less distinguishable spatial structures from the canopy,
280 and a peak shifted to the larger scales (Fig. 4), i.e. NDVI does not distinguish smaller spatial structures. At much larger
281 scales (>100-200 m), the vegetation indicators decline smoothly, while NDVI and especially lidar show an increase
282 in variance probably associated with topographic heterogeneity.

283 One reason why vegetation indicators and LiDAR captured variability at spatial scales larger than the most
284 common tree crown sizes on BCI is that canopy heights tend to be more uniform on BCI compared to other tropical
285 forests, possibly due to wind (Bohlman and O'Brien, 2006). For example, Dipterocarpus dominated South-East Asian
286 forests have emergent trees, unlike BCI, which can reach up to 60 m in height. Additionally, tree crowns on BCI tend
287 to be more flat-topped than conical or rounded, and trees can be found clumped in similar heights, which could explain
288 why the most often detected unit is larger than the mean of a single crown. On the other end of the spectrum, forest
289 gaps can be larger than a single crown because treefall often affects neighbouring trees.

290 Vegetation indicators and the Lidar-derived surface model represent the spectral and structural properties most
291 broadly of the upper canopy, and thus it is conceivable that they display similar spatial variability. However, NIRv,
292 FCVI, NIRvrad, and EVI discriminated details at a different spatial scale from NDVI and LiDAR. These results
293 parallel the variability detected in their distributions (Fig. 3 and Table A1), where NDVI patterns were distinct from
294 the other vegetation indicators. Taken together, these results show that NIRv, FCVI, and NIRvrad have a smoother
295 spatial pattern and peak at finer scales than NDVI, which is known to saturate at high green biomass (Zhu and Liu,
296 2015; Huete et al., 2002), whereas the emerging vegetation indicators should better correlate with aspects of
297 photosynthetic capacity. Thus, these emerging indicators should measure finer resolution spatial heterogeneity and
298 should be more adept at monitoring changes in structure and function of the canopy than NDVI. Additionally, the
299 emerging indicators can potentially disaggregate the physiological and structural component of SIF when SIF
300 measurements are available since changes in structure of the forest coincide with changes in GPP (Wang et al., 2020;
301 Wu et al., 2020; Yang et al., 2020; Dechant et al., 2020). Emerging indicators' heightened ability to differentiate the
302 fine-scale spatial variability in the canopy is likely due to the influence of high upwelling of NIR from the canopy and
303 understory, particularly in the dry season, which tend to blur the signal of the upper canopy for NDVI. Notably, EVI
304 and NDVI, two common indicators of vegetation greenness, show differences in their power spectrum, in particular
305 the slope of the curve for scales less than 20 m. EVI was designed to better capture vegetation changes by exploiting
306 variability in the reflectance in the blue range, especially effective in dense green canopies. This may help explain the
307 scale of variability in this canopy where variation in the blue may be expected to manifest, especially because

308 deciduous crowns, which have high reflectance in blue wavelengths compared to fully leaved crowns, are present on
309 BCI.
310

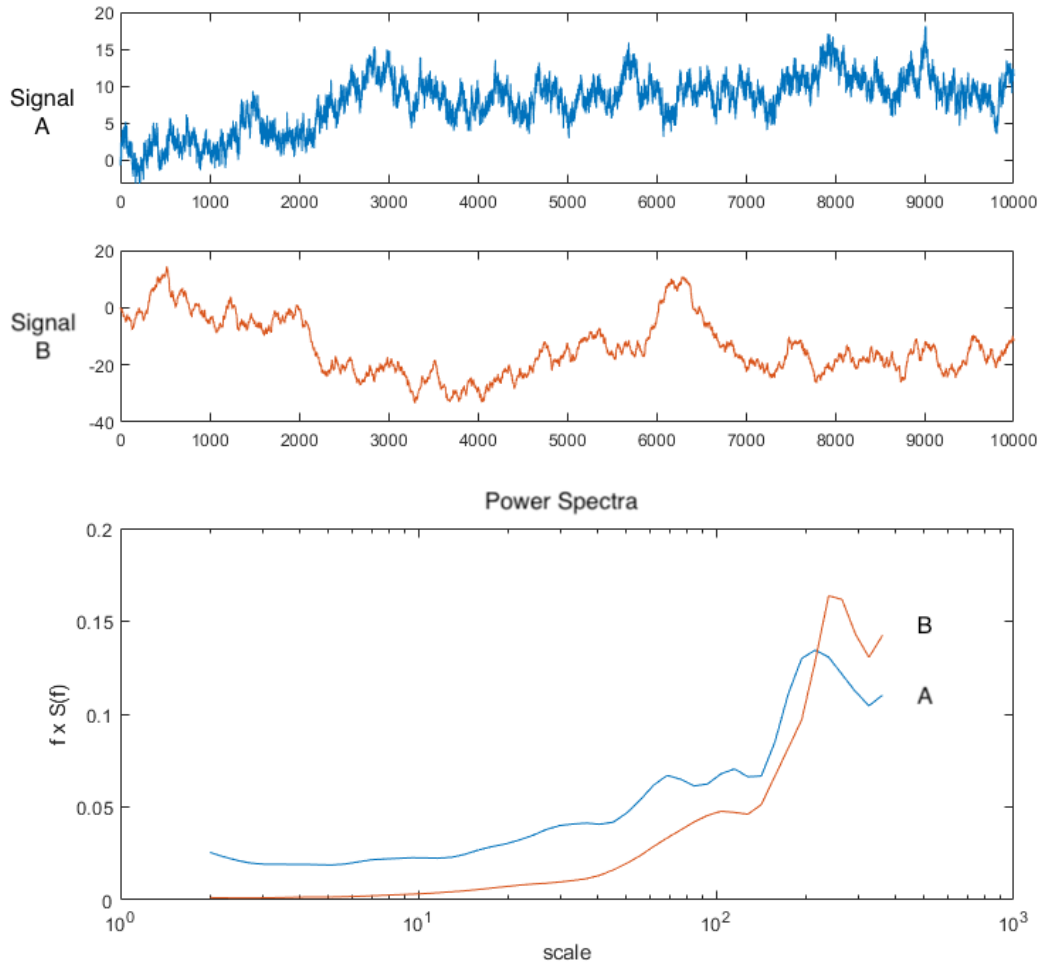


311
312 **Fig. 4. Ensemble wavelet power spectra for all the quantities used in this study and a LiDAR-derived digital**
313 **surface model (DSM). Note that FCVI and NIRv are similar, thus the NIRv curve is obscured by the FCVI.**
314 **Ensembles were created by averaging the spectrum of individual transects, then averaging across flights. Note**
315 **that in this representation, the spectrum divided by the corresponding scale as a function of the log of the scale,**
316 **the area beneath the curve is proportional to the variance.**

317 4 Conclusions

318 We examined NIRv, FCVI, and NIRvrad, emerging vegetation indicators related to fPAR and the scattering of
319 SIF photons, of a semi-deciduous tropical forest canopy using UAS-based hyperspectral data. Our findings
320 demonstrate that NIRvrad has greater potential to track GPP over the course of a day than the non-radiance-based
321 indices as evidenced by a shared correlation among NIRvrad, PAR, and GPP. Thus NIRvrad is a potential proxy for
322 tracking GPP on short timescales without the need for separate measurements of incoming irradiance, which SIF
323 requires. Also, NIRv, FCVI, and NIRvrad at high spatial resolution (~15cm) unveil greater spatial and diurnal
324 variability of BCI's tropical forest canopy versus EVI or NDVI, which may pave the way to improve our understanding
325 of the relationship between GPP and remote sensing observations. The dominant scale driving spatial variability of
326 spectral measurements and lidar data are larger forest structures occurring on BCI, such as groups of similar trees or
327 forest gaps. Yet, smaller, broader peaks in the power spectra of NIRv, FCVI, NIRvrad, and EVI indicate these four
328 indices incorporate smaller scale information compared to NDVI. Taken together, the demonstrated potential to track
329 GPP, measure spatial heterogeneity and variability, and capture forest structural characteristics of BCI open greater
330 possibilities to examine structure and function within and across this tropical forest.

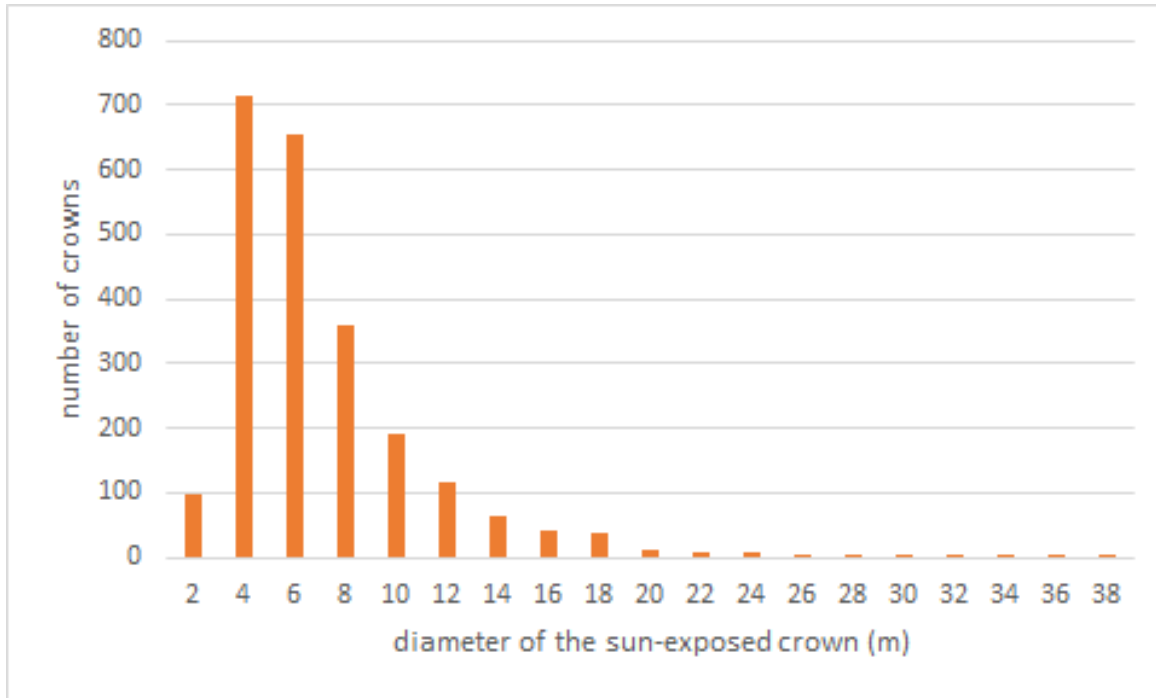
331 Because remote sensing advancements are making it possible to capture physiological responses of vegetation,
332 the importance of improved techniques to examine the radiation regime, for instance estimating fPAR or APAR, can
333 be overlooked. However, recent studies have highlighted the importance and difficulties of measuring fPAR and
334 APAR, the strong dependence of measurements on illumination and viewing geometry, as well as the need for
335 increased understanding of structure-related radiation regime information more generally e.g. (Hao et al., 2021;
336 Dechant et al., 2020; Baldocchi et al., 2020; Rocha et al., 2021; Zhang et al., 2020). For NIRv, FCVI, and NIRvrad,
337 inclusion of the NIR spectral region makes the emerging indices more sensitive to incoming, absorbed, and scattered
338 radiation, which can be influenced by illumination and viewing geometry, changes in canopy leaf angles or associated
339 structure changes. In the case of NIRvrad, which was most strongly associated with GPP, changes in light regime and
340 associated photosynthetic capacity can even be captured diurnally. This study highlights the importance of
341 understanding the incoming solar radiation, absorbed and scattered radiation, and illumination and viewing geometry
342 of any remote sensing data, but it also encourages exploiting RS observations to improve our ability to measure
343 structure-related light capture and scattering patterns. It is in this role, we show these measurements should be further
344 investigated as valuable tools to improve our understanding of complex tropical forest canopies and potentially as an
345 improved estimate of fPAR, APAR, or GPP. While this study focuses on BCI, these techniques could be applied more
346 broadly for the purposes of defining the dominant scale of spatial variability, tracking structural changes, monitoring
347 coincident changes in GPP or light regime, or as inputs to vegetation models of tropical forest structure and function.



349

350 **Figure A1.** Sample signals with relatively higher noise (Signal A) and lower noise (Signal B) and their corresponding
 351 **Power Spectra** ensemble plotted as normalized on log scale. Note the representation of the variance by area under the curve
 352 is preserved by multiplying the Power ($S(f)$) by the frequency (f). In this way the area beneath the curve is still proportional
 353 to the variance.

354



355

356 **Figure A2.** Distribution of tree crown sizes on BCI in a sample ~10 ha plot taken from digitized high spatial resolution
 357 stereo photos that were linked to stems in the field (Bohman and Pacala 2012). This ~10 ha plot does not coincide with the
 358 ~10 ha area sampled by the UAS near the eddy covariance tower in this study.

359

360 **Table A1.** Mean, standard deviation (Sdev) and coefficient of variation (CV) of NIRv, NIRvrad, and FCVI measurements
 361 for the study.

362

Flight Time	Mean NIRv	SDev NIRv	CV NIRv (%)	Mean NIRvrad	SDev NIRvrad	CV NIRvrad (%)	Mean FCVI	SDev FCVI	CV FCVI (%)
Jan30_1000	0.26	0.16	61.36	0.60	0.36	60.54	0.29	0.18	59.69
Jan30_1100	0.24	0.15	61.48	0.54	0.33	60.56	0.27	0.16	60.89
Jan30_1200	0.29	0.15	49.20	0.82	0.39	47.59	0.34	0.16	47.88
Jan30_1330	0.28	0.14	50.46	0.81	0.40	49.24	0.32	0.16	49.16
Jan30_1430	0.27	0.15	55.46	0.70	0.38	54.38	0.31	0.17	54.22
Jan30_1530	0.21	0.14	65.10	0.63	0.41	64.71	0.25	0.16	64.01
Jan30_1630	0.16	0.14	91.54	0.32	0.30	91.54	0.17	0.15	91.39
Jan31_0900	0.22	0.14	66.31	0.52	0.34	65.25	0.25	0.16	66.01
Jan31_1000	0.24	0.14	59.43	0.66	0.39	58.29	0.27	0.16	59.04
Jan31_1230	0.30	0.14	47.17	1.09	0.50	45.63	0.35	0.16	45.91
Jan31_1330	0.22	0.14	61.91	0.82	0.51	61.47	0.25	0.15	60.53
Jan31_1430	0.16	0.14	85.32	0.50	0.42	83.81	0.19	0.16	83.83

Jan31_1530	0.86	0.08	9.83	0.61	0.12	20.24	0.53	0.04	8.15
------------	------	------	------	------	------	-------	------	------	------

363
364
365

Table A2. Mean, standard deviation (Sdev) and coefficient of variation (CV) of NDVI and EVI measurements for the study.

Flight Time	Mean NDVI	SDev NDVI	CV NDVI (%)	Mean EVI	SDev EVI	CV EVI (%)
Jan30_1000	0.86	0.10	11.64	0.57	0.18	31.54
Jan30_1100	0.88	0.09	10.15	0.57	0.14	24.40
Jan30_1200	0.85	0.09	10.38	0.52	0.15	28.48
Jan30_1330	0.85	0.09	10.60	0.59	0.15	25.24
Jan30_1430	0.85	0.09	10.35	0.61	0.16	26.84
Jan30_1530	0.85	0.11	12.52	0.54	0.19	35.21
Jan30_1630	0.93	0.06	6.69	0.49	0.18	36.90
Jan31_0900	0.87	0.10	11.54	0.51	0.19	37.24
Jan31_1000	0.87	0.10	11.08	0.55	0.19	34.66
Jan31_1230	0.85	0.08	9.82	0.66	0.15	22.72
Jan31_1330	0.85	0.09	10.70	0.55	0.19	33.80
Jan31_1430	0.85	0.09	10.58	0.42	0.18	43.07
Jan31_1530	0.86	0.08	9.83	0.61	0.12	20.24

366
367
368
369
370

371 ***Code availability***

372 ***Data availability***

373 GatorEye data related to this project can be downloaded from www.gatoreye.org. Code and other material
374 with links provided upon request (repository forthcoming).

375

376 ***Author contributions***

377 T.M. designed the study with the help of S.P. and S.A.B.. M.D. and T.M. outfitted the tower and collected tower-
378 based data, T.M. and E.N.B. collected the UAS data. E.N.B., A.M.A.Z., and T.M. pre-processed the hyperspectral and
379 lidar data. T.M. and M.D. further processed UAV, lidar, and GPP data and ran data analysis. M.D., S.P., S.A.B., C.S.,
380 contributed with the methodological framework, data processing analysis and write up T.M., M.D., S.P., S.A.B., C.S.,

381 E.N.B., and A.M.A.Z. contributed to the interpretation, quality control and revisions of the manuscript. All authors
382 read and approved the final version of the manuscript.

383 ***Competing interests***

384 The authors declare no conflict of interest.

385 ***Acknowledgments***

386 Support for this project, including portions of field logistic and data collection costs and materials, and
387 support for T.M., was provided by the Provost's Postdoctoral Fellows Program at Florida State University. E.N.B.
388 was supported through the School of Forest, Fisheries and Geomatics Sciences, A.M.A.Z through the Center for Latin
389 American Studies, and hardware, software, and system costs associated with the GatorEye and data collection were
390 provided through the McIntire Stennis Program of the USDA and the School of Forest, Fisheries and Geomatics
391 Sciences. M.D. was supported by the Carbon Mitigation Initiative at Princeton University. The authors wish to thank
392 the vast support of the collaborators, staff, and researchers at the Smithsonian Tropical Research Institute and,
393 specifically at Barro Colorado Island, without which this research would not be possible. Among other contributors
394 to the work, we also extend special thanks to Alfonso Zambrano, Carli Merrick, Riley Fortier, and Pete Kerby-Miller
395 for field work assistance, and Dr. S. Joseph Wright and Dr. Helene Muller-Landau for support on site as well.

396

397 **References**

- 398 Alonso, L., Moreno, J., Moya, I., and R. Miller, J. R.: A Comparison of Different Techniques for Passive Measurement
399 of Vegetation Photosynthetic Activity: Solar-Induced Fluorescence, Red-Edge Reflectance Structure and
400 Photochemical Reflectance Indices, *IEEE*, 3, 2003.
- 401 Alonso, L., Gómez-Chova, L., Vila-Francés, J., Amorós-López, J., Guanter, L., Calpe, J., and Moreno, J.: Sensitivity
402 analysis of the Fraunhofer Line Discrimination method for the measurement of chlorophyll fluorescence using a field
403 spectroradiometer, *IEEE*, 4, 2007.
- 404 Alonso, L., Gómez-Chova, L., Vila-Francés, J., Amorós-López, J., Guanter, L., Calpe, J., and Moreno, J.: Improved
405 Fraunhofer Line Discrimination Method for Vegetation Fluorescence Quantification, *IEEE GEOSCIENCE AND
406 REMOTE SENSING LETTERS*, 5, 5, 2008.
- 407 Badgley, G., Field, C. B., and Berry, J. A.: Canopy near-infrared reflectance and terrestrial photosynthesis, *Sci Adv*,
408 3, e1602244, 10.1126/sciadv.1602244, 2017.
- 409 Badgley, G., Anderegg, L. D. L., Berry, J. A., and Field, C. B.: Terrestrial gross primary production: Using NIRV to
410 scale from site to globe, *Glob Chang Biol*, 25, 3731-3740, 10.1111/gcb.14729, 2019.
- 411 Baldocchi, D. D., Ryu, Y., Dechant, B., Eichelmann, E., Hemes, K., Ma, S., Rey Sanchez, C., Shortt, R., Szutu, D.,
412 Valach, A., Verfaillie, J., Badgley, G., Zeng, Y., and Berry, J. A.: Outgoing Near Infrared Radiation from Vegetation
413 Scales with Canopy Photosynthesis Across a Spectrum of Function, Structure, Physiological Capacity and Weather,
414 *Journal of Geophysical Research: Biogeosciences*, 10.1029/2019jg005534, 2020.
- 415 Berry, Z. C., & Goldsmith, G. R.: Diffuse light and wetting differentially affect tropical tree leaf photosynthesis. *New
416 Phytologist*, 225(1), 143-153, 10.1111/nph.16121, 2020.
- 417 Bohlman, S. and O'Brien, S.: Allometry, adult stature and regeneration requirement of 65 tree species on Barro
418 Colorado Island, Panama, *Journal of Tropical Ecology*, 22, 123-136, 10.1017/s0266467405003019, 2006.
- 419 Bohlman, S. and Pacala, S.: A forest structure model that determines crown layers and partitions growth and mortality
420 rates for landscape-scale applications of tropical forests, *Journal of Ecology*, 100, 508-518, 10.1111/j.1365-
421 2745.2011.01935.x, 2012.

422 Castro, A. O., Chen, J., Zang, C. S., Shekhar, A., Jimenez, J. C., Bhattacharjee, S., Kindu, M., Morales, V. H., and
423 Rammig, A.: OCO-2 Solar-Induced Chlorophyll Fluorescence Variability across Ecoregions of the Amazon Basin
424 and the Extreme Drought Effects of El Niño (2015–2016), *Remote Sensing*, 12, 10.3390/rs12071202, 2020.

425 Clark, D. B., Olivas, P. C., Oberbauer, S. F., Clark, D. A., and Ryan, M. G.: First direct landscape-scale measurement
426 of tropical rain forest Leaf Area Index, a key driver of global primary productivity, *Ecol Lett*, 11, 163-172,
427 10.1111/j.1461-0248.2007.01134.x, 2008.

428 Clark, D. A., Asao, S., Fisher, R., Reed, S., Reich, P. B., Ryan, M. G., Wood, T. E., and Yang, X.: Reviews and
429 syntheses: Field data to benchmark the carbon cycle models for tropical forests, *Biogeosciences*, 14, 4663-4690,
430 10.5194/bg-14-4663-2017, 2017.

431 Cogliati, S., Verhoef, W., Kraft, S., Sabater, N., Alonso, L., Vicent, J., Moreno, J., Drusch, M., and Colombo, R.:
432 Retrieval of sun-induced fluorescence using advanced spectral fitting methods, *Remote Sensing of Environment*, 169,
433 344-357, 10.1016/j.rse.2015.08.022, 2015.

434 Condit, R. S., Watts, K., Bohlman, S., Perez, R., Foster, R. B., and Hubbell, S. P.: Quantifying the deciduousness of
435 tropical forest canopies under varying climates, *Journal of Vegetation Science*, 11, 10, 2000.

436 Dechant, B., Ryu, Y., Badgley, G., Zeng, Y., Berry, J. A., Zhang, Y., Goulas, Y., Li, Z., Zhang, Q., Kang, M., Li, J.,
437 and Moya, I.: Canopy structure explains the relationship between photosynthesis and sun-induced chlorophyll
438 fluorescence in crops, *Remote Sensing of Environment*, 241, 10.1016/j.rse.2020.111733, 2020.

439 Detto, M., Baldocchi, D., and Katul, G. G.: Scaling Properties of Biologically Active Scalar Concentration
440 Fluctuations in the Atmospheric Surface Layer over a Managed Peatland, *Boundary-Layer Meteorology*, 136, 407-
441 430, 10.1007/s10546-010-9514-z, 2010.

442 Detto, M., Wright, S. J., Calderon, O., and Muller-Landau, H. C.: Resource acquisition and reproductive strategies of
443 tropical forest in response to the El Niño-Southern Oscillation, *Nature communications*, 9, 913, 10.1038/s41467-018-
444 03306-9, 2018.

445 Frankenberg, C., Fisher, J. B., Worden, J. R., Badgley, G., Saatchi, S. S., Lee, J. E., Toon, G. C., Butz, A., Jung, M.,
446 Kuze, A., and Yokota, T.: New global observations of the terrestrial carbon cycle from GOSAT: Patterns of plant
447 fluorescence with gross primary productivity, *Geophysical Research Letters*, 38, 10.1029/2011gl048738, 2011.

448 Gamon, J. A., Kovalchuck, O., Wong, C. Y. S., Harris, A., and Garrity, S. R.: Monitoring seasonal and diurnal changes
449 in photosynthetic pigments with automated PRI and NDVI sensors, *Biogeosciences*, 12, 4149-4159, 10.5194/bg-12-
450 4149-2015, 2015.

451 Gao, W., Kim, Y., Ustin, S. L., Huete, A. R., Jiang, Z., and Miura, T.: Multisensor reflectance and vegetation index
452 comparisons of Amazon tropical forest phenology with hyperspectral Hyperion data, *Remote Sensing and Modeling
453 of Ecosystems for Sustainability IV*, 10.1117/12.734974, 2007.

454 Gelybó, G., Barcza, Z., Kern, A., and Kljun, N.: Effect of spatial heterogeneity on the validation of remote sensing
455 based GPP estimations, *Agricultural and Forest Meteorology*, 174-175, 43-53, 10.1016/j.agrformet.2013.02.003,
456 2013.

457 Glenn, E. P., Huete, A. R., Nagler, P. L., and Nelson, S. G.: Relationship Between Remotely-sensed Vegetation
458 Indices, Canopy Attributes and Plant Physiological Processes: What Vegetation Indices Can and Cannot Tell Us About
459 the Landscape, *Sensors*, 8, 24, 2008.

460 Guan, K., Pan, M., Li, H., Wolf, A., Wu, J., Medvigy, D., Caylor, K. K., Sheffield, J., Wood, E. F., Malhi, Y., Liang,
461 M., Kimball, J. S., Saleska, Scott R., Berry, J., Joiner, J., and Lyapustin, A. I.: Photosynthetic seasonality of global
462 tropical forests constrained by hydroclimate, *Nature Geoscience*, 8, 284-289, 10.1038/ngeo2382, 2015.

463 Guanter, L., Frankenberg, C., Dudhia, A., Lewis, P. E., Gómez-Dans, J., Kuze, A., Suto, H., and Grainger, R. G.:
464 Retrieval and global assessment of terrestrial chlorophyll fluorescence from GOSAT space measurements, *Remote
465 Sensing of Environment*, 121, 236-251, 10.1016/j.rse.2012.02.006, 2012.

466 Guanter, L., Zhang, Y., Jung, M., Joiner, J., Voigt, M., Berry, J. A., Frankenberg, C., Huete, A. R., Zarco-Tejada, P.,
467 Lee, J. E., Moran, M. S., Ponce-Campos, G., Beer, C., Camps-Valls, G., Buchmann, N., Gianelle, D., Klumpp, K.,
468 Cescatti, A., Baker, J. M., and Griffis, T. J.: Global and time-resolved monitoring of crop photosynthesis with
469 chlorophyll fluorescence, *Proceedings of the National Academy of Sciences of the United States of America*, 111,
470 E1327-1333, 10.1073/pnas.1320008111, 2014.

471 Hao, D., Asrar, G. R., Zeng, Y., Yang, X., Li, X., Xiao, J., Guan, K., Wen, J., Xiao, Q., Berry, J. A., and Chen, M.:
472 Potential of hotspot solar-induced chlorophyll fluorescence for better tracking terrestrial photosynthesis, *Glob Chang
473 Biol*, 10.1111/gcb.15554, 2021.

474 Heinsch, F. A., Maosheng, Z., Running, S. W., Kimball, J. S., Nemani, R. R., Davis, K. J., Bolstad, P. V., Cook, B.
475 D., Desai, A. R., Ricciuto, D. M., Law, B. E., Oechel, W. C., Hyojung, K., Hongyan, L., Wofsy, S. C., Dunn, A. L.,
476 Munger, J. W., Baldocchi, D. D., Liukang, X., Hollinger, D. Y., Richardson, A. D., Stoy, P. C., Siqueira, M. B. S.,
477 Monson, R. K., Burns, S. P., and Flanagan, L. B.: Evaluation of remote sensing based terrestrial productivity from

478 MODIS using regional tower eddy flux network observations, *IEEE Transactions on Geoscience and Remote Sensing*,
479 44, 1908-1925, 10.1109/tgrs.2005.853936, 2006.

480 Huete, A., Didan, K., Miura, T., Rodriguez, E. P., Gao, X., and Ferreira, L. G.: Overview of the radiometric and
481 biophysical performance of the MODIS vegetation indices, *Remote Sensing of Environment*, 83, 19, 2002.

482 Huete, A. R., Restrepo-Coupe, N., Ratana, P., Didan, K., Saleska, S. R., Ichii, K., Panuthai, S., and Gamo, M.: Multiple
483 site tower flux and remote sensing comparisons of tropical forest dynamics in Monsoon Asia, *Agricultural and Forest
484 Meteorology*, 148, 748-760, 10.1016/j.agrformet.2008.01.012, 2008.

485 Jiang, Z., Huete, A., Didan, K., and Miura, T.: Development of a two-band enhanced vegetation index without a blue
486 band, *Remote Sensing of Environment*, 112, 3833-3845, 10.1016/j.rse.2008.06.006, 2008.

487 Joiner, J., Yoshida, Y., Vasilkov, A. P., Yoshida, Y., Corp, L. A., and Middleton, E. M.: First observations of global
488 and seasonal terrestrial chlorophyll fluorescence from space, *Biogeosciences*, 8, 637-651, 10.5194/bg-8-637-2011,
489 2011.

490 Julitta, T.: Optical proximal sensing for vegetation monitoring, PhD Dissertation, Department of Earth and
491 Environmental Sciences, University of Milano-Bicocca, 136 pp., 2015.

492 Jung, M., Reichstein, M., Margolis, H. A., Cescatti, A., Richardson, A. D., Arain, M. A., Arneth, A., Bernhofer, C.,
493 Bonal, D., Chen, J., Gianelle, D., Gobron, N., Kiely, G., Kutsch, W., Lasslop, G., Law, B. E., Lindroth, A., Merbold,
494 L., Montagnani, L., Moors, E. J., Papale, D., Sottocornola, M., Vaccari, F., and Williams, C.: Global patterns of land-
495 atmosphere fluxes of carbon dioxide, latent heat, and sensible heat derived from eddy covariance, satellite, and
496 meteorological observations, *Journal of Geophysical Research*, 116, 10.1029/2010jg001566, 2011.

497 Köhler, P., Guanter, L., Kobayashi, H., Walther, S., and Yang, W.: Assessing the potential of sun-induced fluorescence
498 and the canopy scattering coefficient to track large-scale vegetation dynamics in Amazon forests, *Remote Sensing of
499 Environment*, 769-785, 10.1016/j.rse.2017.09.025, 2017.

500 Lasslop, G., Reichstein, M., Detto, M., Richardson, A. D., and Baldocchi, D. D.: Comment on Vickers et al.: Self-
501 correlation between assimilation and respiration resulting from flux partitioning of eddy-covariance CO₂ fluxes,
502 *Agricultural and Forest Meteorology*, 150, 312-314, 10.1016/j.agrformet.2009.11.003, 2010.

503 Laurance, W. F., Uuseche, D. C., Rendeiro, J., Kalka, M., Bradshaw, C. J., Sloan, S. P., Laurance, S. G., Campbell, M.,
504 Abernethy, K., Alvarez, P., Arroyo-Rodriguez, V., Ashton, P., Benitez-Malvido, J., Blom, A., Bobo, K. S., Cannon,
505 C. H., Cao, M., Carroll, R., Chapman, C., Coates, R., Cords, M., Danielsen, F., De Dijn, B., Dinerstein, E., Donnelly,
506 M. A., Edwards, D., Edwards, F., Farwig, N., Fashing, P., Forget, P. M., Foster, M., Gale, G., Harris, D., Harrison,
507 R., Hart, J., Karpanty, S., Kress, W. J., Krishnaswamy, J., Logsdon, W., Lovett, J., Magnusson, W., Maisels, F.,
508 Marshall, A. R., McClearn, D., Mudappa, D., Nielsen, M. R., Pearson, R., Pitman, N., van der Ploeg, J., Plumptre, A.,
509 Poulsen, J., Quesada, M., Rainey, H., Robinson, D., Roetgers, C., Rovero, F., Scatena, F., Schulze, C., Sheil, D.,
510 Struhsaker, T., Terborgh, J., Thomas, D., Timm, R., Urbina-Cardona, J. N., Vasudevan, K., Wright, S. J., Arias, G. J.,
511 Arroyo, L., Ashton, M., Auzel, P., Babaasa, D., Babweteera, F., Baker, P., Banki, O., Bass, M., Bila-Isia, I., Blake,
512 S., Brockelman, W., Brokaw, N., Bruhl, C. A., Bunyavejchewin, S., Chao, J. T., Chave, J., Chellam, R., Clark, C. J.,
513 Clavijo, J., Congdon, R., Corlett, R., Dattaraja, H. S., Dave, C., Davies, G., Beisiegel Bde, M., da Silva Rde, N., Di
514 Fiore, A., Diesmos, A., Dirzo, R., Doran-Sheehy, D., Eaton, M., Emmons, L., Estrada, A., Ewango, C., Fedigan, L.,
515 Feer, F., Fruth, B., Willis, J. G., Goodale, U., Goodman, S., Guix, J. C., Guthiga, P., Haber, W., Hamer, K., Herbinger,
516 I., Hill, J., Huang, Z., Sun, I. F., Ickes, K., Itoh, A., Ivanauskas, N., Jackes, B., Janovec, J., Janzen, D., Jiangming, M.,
517 Jin, C., Jones, T., Justiniano, H., Kalko, E., Kasangaki, A., Killeen, T., King, H. B., Klop, E., Knott, C., Kone, I.,
518 Kudavidanage, E., Ribeiro, J. L., Lattke, J., Laval, R., Lawton, R., Leal, M., Leighton, M., Lentino, M., Leonel, C.,
519 Lindsell, J., Ling-Ling, L., Linsenmair, K. E., Losos, E., Lugo, A., Lwanga, J., Mack, A. L., Martins, M., McGraw,
520 W. S., McNab, R., Montag, L., Thompson, J. M., Nabe-Nielsen, J., Nakagawa, M., Nepal, S., Norconk, M., Novotny,
521 V., O'Donnell, S., Opiang, M., Ouboter, P., Parker, K., Parthasarathy, N., Pisciotta, K., Prawiradilaga, D., Pringle, C.,
522 Rajathurai, S., Reichard, U., Reinartz, G., Renton, K., Reynolds, G., Reynolds, V., Riley, E., Rodel, M. O., Rothman,
523 J., Round, P., Sakai, S., Sanaïotti, T., Savini, T., Schaab, G., Seidensticker, J., Siaka, A., Silman, M. R., Smith, T. B.,
524 de Almeida, S. S., Sodhi, N., Stanford, C., Stewart, K., Stokes, E., Stoner, K. E., Sukumar, R., Surbeck, M., Tobler,
525 M., Tschardtke, T., Turkalo, A., Umapathy, G., van Weerd, M., Rivera, J. V., Venkataraman, M., Venn, L., Vereza,
526 C., de Castilho, C. V., Waltert, M., Wang, B., Watts, D., Weber, W., West, P., Whitacre, D., Whitney, K., Wilkie, D.,
527 Williams, S., Wright, D. D., Wright, P., Xiankai, L., Yonzon, P., and Zamzani, F.: Averting biodiversity collapse in
528 tropical forest protected areas, *Nature*, 489, 290-294, 10.1038/nature11318, 2012.

529 Lee, J. E., Frankenberg, C., van der Tol, C., Berry, J. A., Guanter, L., Boyce, C. K., Fisher, J. B., Morrow, E., Worden,
530 J. R., Asefi, S., Badgley, G., and Saatchi, S.: Forest productivity and water stress in Amazonia: observations from
531 GOSAT chlorophyll fluorescence, *Proceedings. Biological sciences / The Royal Society*, 280, 20130171,
532 10.1098/rspb.2013.0171, 2013.

533 Lewis, S. L., Lloyd, J., Sitch, S., Mitchard, E. T. A., and Laurance, W. F.: Changing Ecology of Tropical Forests:
534 Evidence and Drivers, *Annual Review of Ecology, Evolution, and Systematics*, 40, 529-549,
535 10.1146/annurev.ecolsys.39.110707.173345, 2009.

536 Liangyun Liu, X. L., ZhihuiWang, and Bing Zhang: Measurement and Analysis of BidirectionalSIF Emissions in
537 Wheat Canopies, *IEEE TRANSACTIONS ON GEOSCIENCE AND REMOTE SENSING*, 12, 2016.

538 Liu, J., Bowman, K. W., Schimel, D. S., Parazoo, N. C., Jiang, Z., Lee, M., Bloom, A. A., Wunch, D., Frankenberg,
539 C., Sun, Y., O'Dell, C. W., Gurney, K. R., Menemenlis, D., Gierach, M., Crisp, D., and Eldering, A.: Contrasting
540 carbon cycle responses of the tropical continents to the 2015-2016 El Nino, *Science*, 358, eaam5690,
541 10.1126/science.aam5690, 2017.

542 Liu, L., Yang, X., Gong, F., Su, Y., Huang, G., and Chen, X.: The Novel Microwave Temperature Vegetation Drought
543 Index (MTVDI) Captures Canopy Seasonality across Amazonian Tropical Evergreen Forests, *Remote Sensing*, 13,
544 10.3390/rs13030339, 2021.

545 Liu, X., Liu, L., Zhang, S., and Zhou, X.: New Spectral Fitting Method for Full-Spectrum Solar-Induced Chlorophyll
546 Fluorescence Retrieval Based on Principal Components Analysis, *Remote Sensing*, 7, 10626-10645,
547 10.3390/rs70810626, 2015.

548 Logan, B. A., Adams, W. W., and Demmig-Adams, B.: Viewpoint:Avoiding common pitfalls of chlorophyll
549 fluorescence analysis under field conditions, *Functional Plant Biology*, 34, 853, 10.1071/fp07113, 2007.

550 Magney, T. S., Frankenberg, C., Fisher, J. B., Sun, Y., North, G. B., Davis, T. S., Kornfeld, A., and Siebke, K.:
551 Connecting active to passive fluorescence with photosynthesis: a method for evaluating remote sensing measurements
552 of Chl fluorescence, *The New phytologist*, 1594-1608, 10.1111/nph.14662, 2017.

553 Malenovsky, Z., Mishra, K. B., Zemek, F., Rascher, U., and Nedbal, L.: Scientific and technical challenges in remote
554 sensing of plant canopy reflectance and fluorescence, *Journal of experimental botany*, 60, 2987-3004,
555 10.1093/jxb/erp156, 2009.

556 Malhi, Y.: The productivity, metabolism and carbon cycle of tropical forest vegetation, *Journal of Ecology*, 100, 65-
557 75, 10.1111/j.1365-2745.2011.01916.x, 2012.

558 Medlyn, B. E.: Physiological basis of the light use efficiency model, *Tree Physiology*, 18, 167-176,
559 <https://doi.org/10.1093/treephys/18.3.167>, 1998.

560 Meroni, M., Rossini, M., Guanter, L., Alonso, L., Rascher, U., Colombo, R., and Moreno, J.: Remote sensing of solar-
561 induced chlorophyll fluorescence: Review of methods and applications, *Remote Sensing of Environment*, 113, 2037-
562 2051, 10.1016/j.rse.2009.05.003, 2009.

563 Merrick, Pau, Jorge, Bennartz, and Silva: Spatiotemporal Patterns and Phenology of Tropical Vegetation Solar-
564 Induced Chlorophyll Fluorescence across Brazilian Biomes Using Satellite Observations, *Remote Sensing*, 11,
565 10.3390/rs11151746, 2019.

566 Merrick, T., Jorge, M. L. S. P., Silva, T. S. F., Pau, S., Rausch, J., Broadbent, E. N., and Bennartz, R.: Characterization
567 of chlorophyll fluorescence, absorbed photosynthetically active radiation, and reflectance-based vegetation index
568 spectroradiometer measurements, *International Journal of Remote Sensing*, 41, 6755-6782,
569 10.1080/01431161.2020.1750731, 2020.

570 Mitchard, E. T. A.: The tropical forest carbon cycle and climate change, *Nature*, 559, 527-534, 10.1038/s41586-018-
571 0300-2, 2018.

572 Monteith, J.L., Climate and the efficiency of crop production in Britain, *Phil. Trans. R. Soc. Land.*, 281, 277-294,
573 1977.

574 Morton, D. C., Rubio, J., Cook, B. D., Gastellu-Etcheberry, J. P., Longo, M., Choi, H., Hunter, M. O., and Keller, M.:
575 Amazon forest structure generates diurnal and seasonal variability in light utilization, *Biogeosciences Discussions*,
576 12, 19043-19072, 10.5194/bgd-12-19043-2015, 2015.

577 Morton, D. C., Nagol, J., Carabajal, C. C., Rosette, J., Palace, M., Cook, B. D., Vermote, E. F., Harding, D. J., and
578 North, P. R.: Amazon forests maintain consistent canopy structure and greenness during the dry season, *Nature*, 506,
579 221-224, 10.1038/nature13006, 2014.

580 Moya, I., Camenen, L., Evain, S., Goulas, Y., Cerovic, Z. G., Latouche, G., Flexas, J., and Ounis, A.: A new instrument
581 for passive remote sensing1. Measurements of sunlight-induced chlorophyll fluorescence, *Remote Sensing of
582 Environment*, 91, 186-197, 10.1016/j.rse.2004.02.012, 2004.

583 Plascyk, J. A.: The MK II Fraunhofer Line Discriminator (FLD -II) for Airborne and Orbital Remote Sensing of Solar-
584 Stimulated Luminescence, *Optical Engineering*, 14, 8, 1975.

585 Porcar-Castell, A., Tyystjarvi, E., Atherton, J., van der Tol, C., Flexas, J., Pfundel, E. E., Moreno, J., Frankenberg, C.,
586 and Berry, J. A.: Linking chlorophyll a fluorescence to photosynthesis for remote sensing applications: mechanisms
587 and challenges, *Journal of experimental botany*, 65, 4065-4095, 10.1093/jxb/eru191, 2014.

588 R Development Core Team: R: A language and environment for statistical computing, R Foundation for Statistical
589 Computing [code], 2010.

590 Rocha, A. V., Appel, R., Bret-Harte, M. S., Euskirchen, E. S., Salmon, V., and Shaver, G.: Solar position confounds
591 the relationship between ecosystem function and vegetation indices derived from solar and photosynthetically active
592 radiation fluxes, *Agricultural and Forest Meteorology*, 298-299, 10.1016/j.agrformet.2020.108291, 2021.

593 Rong Li, F. Z.: Accuracy assessment on reconstruction algorithms of solar-induced Fluorescence Spectrum,
594 *Geoscience and Remote Sensing Symposium (IGARSS) IEEE International*, 1727-1730,

595 Rossini, M., Alonso, L., Cogliati, S., Damm, A., Guanter, L., Julitta, T., Meroni, M., Moreno, J., Panigada, C., Pinto,
596 F., Rascher, U., Schickling, A., Schüttemeyer, D., Zemek, F., and Colombo, R.: Measuring sun-induced chlorophyll
597 fluorescence: An evaluation and synthesis of existing field data, 5th International workshop on remote sensing of
598 vegetation fluorescence, Paris, France, 1-5,

599 Rouse Jr, J. W., Haas, R. H., Schell, J. A., and Deering, D. W.: Paper A 20, *Third Earth Resources Technology Satellite-*
600 *1 Symposium: The Proceedings of a Symposium Goddard Space Flight Center at Washington, DC 309*,

601 Running, S. W., Nemani, R. R., Heinsch, F. A., Zhao, M., Reeves, M., and Hashimoto, H.: A Continuous Satellite-
602 Derived Measure of Global Terrestrial Primary Production, *BioScience*, 54, 547-551, 2004.

603 Ryu, Y., Jiang, C., Kobayashi, H., and Detto, M.: MODIS-derived global land products of shortwave radiation and
604 diffuse and total photosynthetically active radiation at 5 km resolution from 2000, *Remote Sensing of Environment*,
605 204, 812-825, 10.1016/j.rse.2017.09.021, 2018.

606 Saatchi, S. S., Harris, N. L., Brown, S., Lefsky, M., A., E. T., Mitchare, W. S., Zutta, B. R., Buerman, W., Lewis, S.
607 L., Hagen, S., Petrova, S., White, L., Silman, M., and Morel, A.: Benchmark map of forest carbon stocks in tropical
608 regions across three continents, *Proceedings of the National Academy of Sciences*, 108, 9899-9905, 2010.

609 Saatchi, S. S., Harris, N. L., Brown, S., Lefsky, M., Mitchard, E. T., Salas, W., Zutta, B. R., Buermann, W., Lewis, S.
610 L., Hagen, S., Petrova, S., White, L., Silman, M., and Morel, A.: Benchmark map of forest carbon stocks in tropical
611 regions across three continents, *Proceedings of the National Academy of Sciences of the United States of America*,
612 108, 9899-9904, 10.1073/pnas.1019576108, 2011.

613 Samanta, A., Ganguly, S., and Myneni, R.: MODIS Enhanced Vegetation Index data do not show greening of Amazon
614 forests during the 2005 drought, *New Phytologist*, 189, 4, 2010.

615 Schickling, A., Matveeva, M., Damm, A., Schween, J., Wahner, A., Graf, A., Crewell, S., and Rascher, U.: Combining
616 Sun-Induced Chlorophyll Fluorescence and Photochemical Reflectance Index Improves Diurnal Modeling of Gross
617 Primary Productivity, *Remote Sensing*, 8, 574, 10.3390/rs8070574, 2016.

618 Sims, D., Rahman, A., Cordova, V., Elmasri, B., Baldocchi, D., Bolstad, P., Flanagan, L., Goldstein, A., Hollinger,
619 D., and Misson, L.: A new model of gross primary productivity for North American ecosystems based solely on the
620 enhanced vegetation index and land surface temperature from MODIS, *Remote Sensing of Environment*, 112, 1633-
621 1646, 10.1016/j.rse.2007.08.004, 2008.

622 Springer, K., Wang, R., and Gamon, J. A.: Parallel Seasonal Patterns of Photosynthesis, Fluorescence, and Reflectance
623 Indices in Boreal Trees, *Remote Sensing*, 9, 1-18, 10.3390/rs9070691, 2017.

624 Sun, Y., Frankenberg, C., Wood, J. D., Schimel, D. S., Jung, M., Guanter, L., Drewry, D. T., Verma, M., Porcar-
625 Castell, A., Griffis, T. J., Gu, L., Magney, T. S., Kohler, P., Evans, B., and Yuen, K.: OCO-2 advances photosynthesis
626 observation from space via solar-induced chlorophyll fluorescence, *Science*, 358, eaam5747,
627 10.1126/science.aam5747, 2017.

628 Torrence, C. and Compo, G. P.: A Practical Guide to Wavelet Analysis, *Bulletin of the American Meteorological*
629 *Society*, 79, 61-79, 1998.

630 Tucker, C., Red and photographic infrared linear combinations for vegetation monitoring, *Remote Sensing of*
631 *Environment*, 8, 127-150, 1979.

632 Turner, D. P., Ritts, W. D., Cohen, W. B., Gower, S. T., Zhao, M., Running, S. W., Wofsy, S. C., Urbanski, S., Dunn,
633 A. L., and Munger, J. W.: Scaling Gross Primary Production (GPP) over boreal and deciduous forest landscapes in
634 support of MODIS GPP product validation, *Remote Sensing of Environment*, 88, 256-270, 10.1016/j.rse.2003.06.005,
635 2003.

636 Van Wittenberghe, S., Alonso, L., Verrelst, J., Moreno, J., and Samson, R.: Bidirectional sun-induced chlorophyll
637 fluorescence emission is influenced by leaf structure and light scattering properties — A bottom-up approach, *Remote*
638 *Sensing of Environment*, 158, 169-179, 10.1016/j.rse.2014.11.012, 2015.

639 Van Wittenberghe, S., Alonso, L., Verrelst, J., Hermans, I., Delegido, J., Veroustraete, F., Valcke, R., Moreno, J., and
640 Samson, R.: Upward and downward solar-induced chlorophyll fluorescence yield indices of four tree species as
641 indicators of traffic pollution in Valencia, *Environmental pollution*, 173, 29-37, 10.1016/j.envpol.2012.10.003, 2013.

642 Wang, C., Beringer, J., Hutley, L. B., Cleverly, J., Li, J., Liu, Q., and Sun, Y.: Phenology Dynamics of Dryland
643 Ecosystems Along the North Australian Tropical Transect Revealed by Satellite Solar-Induced Chlorophyll
644 Fluorescence, *Geophysical Research Letters*, 46, 5294-5302, 10.1029/2019gl082716, 2019.

645 Wang, S., Zhang, Y., Ju, W., Qiu, B., and Zhang, Z.: Tracking the seasonal and inter-annual variations of global gross
646 primary production during last four decades using satellite near-infrared reflectance data, *The Science of the total
647 environment*, 755, 142569, 10.1016/j.scitotenv.2020.142569, 2020.

648 Wickham, H.: *ggplot2: Elegant Graphics for Data Analysis*, Springer-Verlag [code], 2016.

649 Wickham, H.: *tidyverse: Easily Install and Load the 'Tidyverse' (R package
650 version 1.2.1) [code]*, 2017.

651 Wickham, H., François, R., Henry, L., and Müller, K.: *dplyr: A Grammar of Data Manipulation (R package version
652 0.7.8) [code]*, 2018.

653 Wright, S. J.: The future of tropical forests, *Ann N Y Acad Sci*, 1195, 1-27, 10.1111/j.1749-6632.2010.05455.x, 2010.

654 Wu, G., Guan, K., Jiang, C., Peng, B., Kimm, H., Chen, M., Yang, X., Wang, S., Suyker, A. E., Bernacchi, C. J.,
655 Moore, C. E., Zeng, Y., Berry, J. A., and Cendrero-Mateo, M. P.: Radiance-based NIRv as a proxy for GPP of corn
656 and soybean, *Environmental Research Letters*, 15, 10.1088/1748-9326/ab65cc, 2020.

657 Xu, L., Saatchi, S. S., Yang, Y., Myneni, R. B., Frankenberg, C., Chowdhury, D., and Bi, J.: Satellite observation of
658 tropical forest seasonality: spatial patterns of carbon exchange in Amazonia, *Environmental Research Letters*, 10,
659 084005, 10.1088/1748-9326/10/8/084005, 2015.

660 Yang, H., Yang, X., Zhang, Y., Heskell, M. A., Lu, X., Munger, J. W., Sun, S., and Tang, J.: Chlorophyll fluorescence
661 tracks seasonal variations of photosynthesis from leaf to canopy in a temperate forest, *Glob Chang Biol*, 23, 2874-
662 2886, 10.1111/gcb.13590, 2017.

663 Yang, J., Tian, H., Pan, S., Chen, G., Zhang, B., and Dangal, S.: Amazon droughts and forest responses: Largely
664 reduced forest photosynthesis but slightly increased canopy greenness during the extreme drought of 2015/2016, *Glob
665 Chang Biol*, 1919-1934, 10.1111/gcb.14056, 2018a.

666 Yang, K., Ryu, Y., Dechant, B., Berry, J. A., Hwang, Y., Jiang, C., Kang, M., Kim, J., Kimm, H., Kornfeld, A., and
667 Yang, X.: Sun-induced chlorophyll fluorescence is more strongly related to absorbed light than to photosynthesis at
668 half-hourly resolution in a rice paddy, *Remote Sensing of Environment*, 216, 658-673, 10.1016/j.rse.2018.07.008,
669 2018b.

670 Yang, P., van der Tol, C., Campbell, P. K. E., and Middleton, E. M.: Fluorescence Correction Vegetation Index
671 (FCVI): A physically based reflectance index to separate physiological and non-physiological information in far-red
672 sun-induced chlorophyll fluorescence, *Remote Sensing of Environment*, 240, 10.1016/j.rse.2020.111676, 2020.

673 Yuan, W., Cai, W., Xia, J., Chen, J., Liu, S., Dong, W., Merbold, L., Law, B., Arain, A., Beringer, J., Bernhofer, C.,
674 Black, A., Blanken, P. D., Cescatti, A., Chen, Y., Francois, L., Gianelle, D., Janssens, I. A., Jung, M., Kato, T., Kiely,
675 G., Liu, D., Marcolla, B., Montagnani, L., Raschi, A., Rouspard, O., Varlagin, A., and Wohlfahrt, G.: Global
676 comparison of light use efficiency models for simulating terrestrial vegetation gross primary production based on the
677 LaThuile database, *Agricultural and Forest Meteorology*, 192-193, 108-120,
678 <https://doi.org/10.1016/j.agrformet.2014.03.007>, 2014.

679 Zarco-Tejada, P. J., González-Dugo, V., and Berni, J. A. J.: Fluorescence, temperature and narrow-band indices
680 acquired from a UAV platform for water stress detection using a micro-hyperspectral imager and a thermal camera,
681 *Remote Sensing of Environment*, 117, 322-337, 10.1016/j.rse.2011.10.007, 2012.

682 Zarco-Tejada, P. J., Morales, A., Testi, L., and Villalobos, F. J.: Spatio-temporal patterns of chlorophyll fluorescence
683 and physiological and structural indices acquired from hyperspectral imagery as compared with carbon fluxes
684 measured with eddy covariance, *Remote Sensing of Environment*, 133, 102-115, 10.1016/j.rse.2013.02.003, 2013.

685 Zarco-Tejada, P. J., Miller, J. R., Mohammed, G. H., Noland, T. L., and Sampson, P. H.: Estimation of chlorophyll
686 fluorescence under natural illumination from hyperspectral data, *International Journal of Applied Earth Observation
687 and Geoinformation*, 3, 7, 2001.

688 Zeng, Y., Badgley, G., Dechant, B., Ryu, Y., Chen, M., and Berry, J. A.: A practical approach for estimating the
689 escape ratio of near-infrared solar-induced chlorophyll fluorescence, *Remote Sensing of Environment*, 232,
690 10.1016/j.rse.2019.05.028, 2019.

691 Zhang, Z., Zhang, Y., Zhang, Q., Chen, J. M., Porcar-Castell, A., Guanter, L., Wu, Y., Zhang, X., Wang, H., Ding,
692 D., and Li, Z.: Assessing bi-directional effects on the diurnal cycle of measured solar-induced chlorophyll fluorescence
693 in crop canopies, *Agricultural and Forest Meteorology*, 295, 10.1016/j.agrformet.2020.108147, 2020.

694 Zhang, Z., Zhang, Y., Zhang, Y., Gobron, N., Frankenberg, C., Wang, S., and Li, Z.: The potential of satellite FPAR
695 product for GPP estimation: An indirect evaluation using solar-induced chlorophyll fluorescence, *Remote Sensing of
696 Environment*, 240, 10.1016/j.rse.2020.111686, 2020.

697 Zhao, M., Running, S., Heinsch, F. A., and Nemani, R.: MODIS-Derived Terrestrial Primary Production, 11, 635-
698 660, 10.1007/978-1-4419-6749-7_28, 2010.
699 Zhu, X. and Liu, D.: Improving forest aboveground biomass estimation using seasonal Landsat NDVI time-series,
700 ISPRS Journal of Photogrammetry and Remote Sensing, 102, 222-231, 10.1016/j.isprsjprs.2014.08.014, 2015.
701
702